Instrumental noise and detectivity analysis of photopyroelectric destructive thermal-wave interferometry

Chinhua Wang and Andreas Mandelis[a)]
Department of Mechanical and Industrial Engineering, Photothermal and Optoelectronic Diagnostics Laboratories, University of Toronto, Toronto M5S 3G8, Canada

(Received 9 November 1999; accepted for publication 13 January 2000)

A complete noise analysis of a two-beam photopyroelectric (thermal-wave) destructive interferometric sensor instrument is presented and compared to its single-beam, noninterferometric counterpart. The noise analysis is performed using a Green-function formalism applied to experimental observations. The instrumental background noise contribution from the detector and the amplifier is separated from the laser noise and the instrumental noise due to amplification associated with different sensitivity scales. The latter serves as the source of comparison between the two sensor configurations. It is found that the dc laser drift noise and low-frequency fluctuation noise, which are dominant in the single-beam mode, are greatly reduced to the same order of magnitude as the instrumental background noise in the two-beam mode. The system white noise resulting from the incident laser beam and from the sensitivity scale (amplification) of the demodulating lock-in amplifier are also examined in light of the experimental data. It is found that the detectivity D^* (the inverse of the noise equivalent power), of the instrument is enhanced by at least 1 order of magnitude in the interferometric mode. © *2000 American Institute of Physics.* [S0034-6748(00)01305-8]

I. INTRODUCTION

A new photothermal technique based on the photopyroelectric (PPE) effect[1] and called ''purely thermal-wave interferometry'' has recently been developed.[2] As already experimentally demonstrated,[3,4] this technique offers an efficient differential methodology for measuring small signal variations in the presence of a large background signal, which can be completely suppressed (i.e., zero baseline signal). The technique experimentally exhibits much enhanced signal dynamic range and much improved detectivity when compared with the conventional single-beam PPE detection configuration. The enhancement of the signal dynamic range is obviously due to the complete suppression of the large baseline signal, which allows for a higher instrumental detectivity than the single-beam configuration. The instrumental sensitivity can be adjusted to the magnitude of the small signal change without being limited by the usually quite large background signal. However, the higher instrumental sensitivity of the two-beam configuration does not measurably affect the magnitude and quality of incident signal and thus the instrumental signal-to-noise ratio (SNR). Furthermore, neither the detectivity D^* nor the SNR can be substantially improved by increasing the instrumental sensitivity of the single-beam configuration in the presence of a large background signal. Therefore, the observed strong improvement of the detectivity in the two-beam configuration must be due to the suppression of the noise level of the system, a fact borne out in all our experiments. This conclusion has motivated us to identify and analyze the relative contributions of noise sources in the system, so as to improve our understanding and optimize the design of our PPE thermal-wave interferometric instrument.

In this article, the noise sources of the PPE setup will be briefly reviewed and a quasiempirical theoretical model will be developed to simulate and compare the relative noise levels between the conventional single-beam mode and the two-beam interferometric mode, respectively.

II. NOISE SOURCES IN A PHOTOPYROELECTRIC SENSOR INSTRUMENT

For quite some time pyroelectric detectors, on which the PPE effect is based, have been extensively studied due to their excellent performance as infrared radiation sensors and their ability to operate under ambient conditions.[5–9] The overall equivalent noise voltage ΔV_N of a pyroelectric system can be expressed as[5]

$$\Delta V_N = (\Delta V_T^2 + \Delta V_J^2 + \Delta V_A^2 + \Delta V_i^2 + \Delta V_0^2)^{1/2}, \tag{1}$$

where ΔV_T represents the spontaneous temperature fluctuation noise about the average temperature in the detector; ΔV_J is the Johnson (thermal) noise[7] associated with the equivalent total resistance of the detecting circuit; ΔV_A and ΔV_i represent, respectively, the voltage noise and the current noise of the amplifier that is connected to the detector; and ΔV_0 is the noise accompanying the incident optical power. The performance of the system is thus evaluated through the noise equivalent power (NEP, $\mathrm{W/Hz^{1/2}}$) and the detectivity (D^*, $\mathrm{cm\,Hz^{1/2}/W}$), which are defined as

$$\mathrm{NEP} = \Delta V_N / \Re_V \tag{2}$$

and

a)Author to whom correspondence should be addressed; electronic mail: mandelis@mie.utoronto.ca

$$D^* = A^{1/2}/\mathrm{NEP}. \tag{3}$$

Here $\Re_V$ is the technical sensitivity of the system.[5,8] It is defined as the ratio of radiant power incident on the system over a corresponding readout of the instrument. For a given instrumental system (the detector and the amplifier), the technical sensitivity of the system is a constant. A is the effective area of the detector (cm^2) receiving the signal-inducing energy. In Eq. (1), the first four noise sources originate in the detector itself and the amplifier circuit system. If the incident energy is assumed to be free of noise (i.e., $\Delta V_0 = 0$), the minimum possible NEP and the maximum possible D^* of the system can be obtained based on the overall noise level determined by the detector and the amplifier *only*. However, in practice, the detectivity of the system is usually much lower than the maximum possible detectivity. One of the reasons is that noise ΔV_0 from the incident energy source is usually much higher than the overall noise generated by the detector and the amplifier, and therefore, it is usually the dominant factor limiting the measurement sensitivity of the system.[10] Much effort has been expended to overcome source noise. The ratio and the subtraction methods using two detectors, or external electronic ratioing/subtracting devices using a single detector, are two frequently used methods. These methods have been successful in reducing the overall noise to a level limited by the detector and amplifier noise, if a specially designed device is employed.[10] From this viewpoint, the recently developed PPE interferometric technique comprises a different measurement scheme, in which a differential measurement is implemented within a single pyroelectric detector in real time, with no need for external ratioing or subtracting device.[2–4]

Comparing the measurement results between the PPE destructive interferometric (differential) two-beam method and its counterpart single-beam configuration, it is recognized that the SNR and D^* improvement in the former scheme must be due to the suppression of laser noise ΔV_0, since all other detector and the amplifier noise sources remain the same in both schemes. Therefore, it becomes important to explain how the two-beam interferometric scheme reduces the incident noise ΔV_0, and drastically improves the detectivity of the measurement over the single-beam method.

III. THEORETICAL ANALYSIS OF PPE SIGNAL AND NOISE GENERATION

A. Modulated PPE output from a PVDF detector

For the purposes of noise analysis, a simple geometry of the essentials of PPE thermal-wave interferometry (TWI) is shown in Fig. 1, in which a pyroelectric polyvinylidene fluoride (PVDF) thin film detector is directly exposed to the ambient gas as shown. Both surfaces of the PVDF detector are coated with metallic coatings used as signal output electrodes. The PPE signal is proportional to the average ac temperature of the PVDF detector.[1] It is governed by the heat conduction equation in the PVDF detector, subject to appropriate boundary conditions. Neglecting radial diffusion effects,[1,2] for the usual case of a broad laser beam waist ($\sim$1 mm) compared to the thermal diffusion length (on the order of microns) in the PVDF,[1,2] the appropriate one-dimensional heat transfer equation has the form:

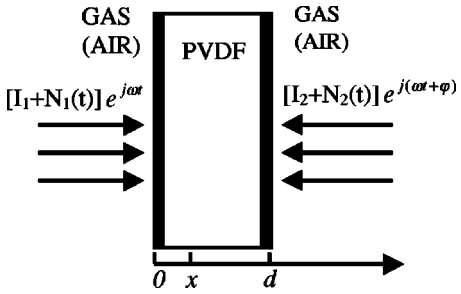

FIG. 1. Geometry of a PPE thermal-wave interferometer for noise and detectivity analysis.

$$\frac{\partial^2 T(x,t)}{\partial x^2} - \frac{1}{\alpha_p}\frac{\partial T(x,t)}{\partial t} = -\frac{S(x,t)}{k_p}, \tag{4}$$

where k_p and α_p are the thermal conductivity and the thermal diffusivity of the PVDF detector, respectively. $S(x,t)$ represents the rate of local thermal power generation per unit volume

$$\begin{aligned} S(x,t) = {} & (1-R_1-A_1)\beta_p[I_1+N_1(t)]\exp(-\beta_p x) \\ & \times \exp(j\omega t) + (1-R_2-A_2)\beta_p[I_2+N_2(t)] \\ & \times \exp[-\beta_p(d-x)]\exp[j(\omega t+\varphi)]. \end{aligned} \tag{5}$$

In Eq. (5), R_1, A_1 and R_2, A_2 are the reflectivity and absorptivity of the front and rear metal-coated surfaces of the PVDF element, respectively; β_p is the optical absorption coefficient of the PVDF (cm^{-1}); I_1, I_2 represent the intensities of the two incident laser beams on opposite sides of the element; $N_1(t)$, $N_2(t)$ are noise sources introduced by each laser beam, expressed as functions of time. The most general boundary conditions at $x=0$ and $x=d$ of the PVDF element are the so-called third-kind boundary conditions

$$k_p\frac{\partial T(x,t)}{\partial n_t} + h_i T(x,t) = h_i T_\infty + f_i(t), \qquad i=1,2 \quad \text{for } x=0 \quad \text{and } d, \tag{6}$$

where h_i is the heat transfer coefficient; T_∞ is the ambient temperature; $f_i(t)$ represents a prescribed heat flux ($\mathrm{W/m}^2$) at the boundary; n_i is an outward normal from the one-dimensional volume of interest, $[0,d]$, at boundary (i). In most of cases, the temperature gradient between the PVDF and the ambient gas is very small, so that the terms proportional to h_i due to convection can be neglected.[11] The terms $(1-R_j-A_j)=T_j$, $j=1,2$ in Eq. (5) represent the bulk transmitted optical power past the metal-coated surfaces. Here T_j is the metal-coated electrode transmittance. The surfaces themselves, however, are sources of thermal-wave production and transport into the bulk of the PVDF sensor by means of their absorptance A_j. These sources are incorporated into the formalism by means of the following boundary conditions:

$$k_p \frac{\partial T}{\partial n_i} = f_i(t), \quad i=1,2 \quad \text{for } x=0 \quad \text{and } d. \tag{7}$$

These constitute boundary conditions of the second kind (Neumann) where, for the case of PPE TWI the front- and back-surface fluxes are, respectively,

$$f_1(t) = A_1[I_1 + N_1(t)]\exp(j\omega t), \tag{8}$$

$$f_2(t) = A_2[I_2 + N_2(t)]\exp[j(\omega t + \varphi)]. \tag{9}$$

Therefore, the boundary conditions at the front and the rear surfaces of the PVDF can be expressed as

$$-k_p \frac{\partial T(x,t)}{\partial x} = A_1[I_1 + N_1(t)]\exp(j\omega t) \quad \text{at } x=0, \tag{10}$$

$$k_p \frac{\partial T(x,t)}{\partial x} = A_2[I_2 + N_2(t)]\exp[j(\omega t + \varphi)] \quad \text{at } x=d. \tag{11}$$

Solving the boundary-value problem defined by Eqs. (4), (10), and (11), the temperature field within the PVDF detector may be derived. Due to the time-dependent nature of the noise sources, $N_1(t)$ and $N_2(t)$, which appear in both heat conduction equation *and* boundary conditions, the method of separation of variables is not applicable. Therefore, the Green-function method is employed to solve this boundary-value problem.

The Green-function solution to the one-dimensional heat conduction in the rectangular coordinate system can be written as[12]

$$T(x,t) = \frac{\alpha_p}{k_p}\int_{\tau=0}^{t} d\tau \int_{x'=0}^{d} S(x',\tau) G(x,t|x',\tau)\, dx'$$

(volume energy generation)

$$+ \alpha_p \int_{\tau=0}^{t} \left[\frac{f_1(\tau)}{k} G(x,t|0,\tau) + \frac{f_2(\tau)}{k} G(x,t|d,\tau) \right] d\tau$$

(boundary conditions/surface energy generation). (12)

In the PPE TWI case, the contribution from the initial-condition term has been neglected due to the periodic heat conduction. $S(x,t)$, and $f_i(t)$, $(i=1,2)$ are given in Eqs. (5), (8), and (9), respectively. $G(x,t|x',\tau)$ in Eq. (12) represents the Green function, which is mathematically unique for a given geometry and a given set of homogenous boundary conditions. For a plate with homogeneous Neumann boundary conditions on both surfaces, the Green function has the following form:[12]

$$G(x,t|x',\tau) = \frac{1}{d}\left[1 + 2\sum_{m=1}^{\infty} e^{-m^2\pi^2\alpha_p(t-\tau)/d^2} \times \cos\left(\frac{m\pi x}{d}\right)\cos\left(\frac{m\pi x'}{d}\right) \right]. \tag{13}$$

Substituting the Green function and the boundary conditions into Eq. (12), we obtain the temperature distribution within the PVDF

$$\begin{aligned} T(x,t) = {} & \frac{\alpha_p}{k_p}\int_{\tau=0}^{t} d\tau \int_{x'=0}^{d} \{(1-R_1-A_1)\beta_p[I_1+N_1(\tau)]e^{j\omega\tau}e^{-\beta_p x'} + (1-R_2-A_2)\beta_p[I_2+N_2(\tau)]e^{j(\omega\tau+\varphi)}e^{-\beta_p(d-x')}\} \\ & \times \frac{1}{d}\left[1 + 2\sum_{m=1}^{\infty} e^{-m^2\pi^2\alpha_p(t-\tau)/d^2}\cos\left(\frac{m\pi x}{d}\right)\cos\left(\frac{m\pi x'}{d}\right)\right] dx' \\ & + \alpha_p \int_{\tau=0}^{t} \left\{ \frac{A_1[I_1+N_1(\tau)]e^{j\omega\tau}}{k_p} \times \frac{1}{d}\left[1 + 2\sum_{m=1}^{\infty} e^{-m^2\pi^2\alpha_p(t-\tau)/d^2}\cos\left(\frac{m\pi x}{d}\right)\right] \right. \\ & \left. + \frac{A_2[I_2+N_2(\tau)]e^{j(\omega\tau+\varphi)}}{k_p} \times \frac{1}{d}\left[1 + 2\sum_{m=1}^{\infty} e^{-m^2\pi^2\alpha_p(t-\tau)/d^2}\cos\left(\frac{m\pi x}{d}\right)\cos(m\pi)\right]\right\} d\tau. \end{aligned} \tag{14}$$

Assuming a short thermal time constant[5] compared with the inverse of the modulation frequency, the output signal from the PVDF detector is the thickness average of the temperature field[1]

$$V_{\mathrm{PVDF}}(\omega,t) = Q_1(\omega)\int_0^d T(x,t,\omega)\, dx, \tag{15}$$

where $Q_1(\omega)$ is an instrumental constant including the physical parameters of the PVDF and the electrical constants of the circuit. After the integration of Eq. (15), the PPE output signal from a PVDF detector is

$$\begin{aligned} V_{\mathrm{PVDF}}(\omega,t) = {} & Q_1(\omega)\frac{\alpha_p}{k_p}\int_{\tau=0}^{t} \{P_1(A_1,R_1,\beta_p) \\ & \times [I_1+N_1(\tau)]e^{j\omega\tau} + P_2(A_2,R_2,\beta_p) \\ & \times [I_2+N_2(\tau)]e^{j(\omega\tau+\varphi)}\}\, d\tau, \end{aligned} \tag{16}$$

where $P_{1,2}(A_{1,2},R_{1,2},\beta_p) = A_{1,2} + (1-e^{-\beta_p d})(1-R_{1,2}-A_{1,2})$ are constants related to surface and bulk optical properties of

the PVDF. Equation (16) provides the desired explicit ac PPE interferometric signal generated by the PVDF detector. This equation shows that the PPE output signal depends on photothermal properties of the PVDF detector, on the intensities of the two incident laser beams, as well as on the corresponding noise sources. The modulated ac signal is then fed into a lock-in amplifier (LIA), a mixer and low-pass filter combination, which demodulates it into amplitude and phase signals.

B. Demodulated PPE signal LIA output

LIAs use a technique known as phase-sensitive detection to single out the component of the signal at a specific reference frequency and phase. Noise signals at frequencies other than the reference frequency are rejected and do not affect the measurement.[13,14] Generally, a LIA contains four main parts: signal input channel, reference channel, multiplier (mixer), and low-pass filter (capacitor–resistor integrator). A modulated periodic noised signal input $s(t)$ is multiplied by (mixed with) a reference signal $r(t)$. This wave form is usually generated internally in digital LIAs. The multiplied product of the signal and the reference is subsequently fed to a low-pass filter to form an averaged and demodulated dc output signal. The operating mechanism of a LIA can be broadly outlined as follows: the noised signal wave form, modulated at frequency ω_1 (amplitude A_s and phase ϕ), is assumed to be accompanied by noise $n(t)$, which could be generated by the sensor element or by the electronics

$$s(t)=[A_s+n(t)]\sin(\omega_1 t+\phi). \tag{17}$$

The reference signal is usually expressed as a sine wave[15] with an angular frequency ω_2:

$$r(t)=A_r \sin \omega_2 t. \tag{18}$$

These two signals are then multiplied and low-pass filtered, resulting in the demodulated output signal $V_{\mathrm{LIA}}(\omega)$ from the LIA.

$$\begin{aligned} V_{\mathrm{LIA}}(\omega,t) &= (1/T_m)\int_0^{T_m} A_r[A_s+n(t)] \\ &\quad \times \sin(\omega_1 t+\phi)\sin(\omega_2 t)\,dt \\ &= (A_s A_r/T_m)\int_0^{T_m} \sin(\omega_1 t+\phi) \\ &\quad \times \sin(\omega_2 t)\,dt + (A_r/T_m) \\ &\quad \times \int_0^{T_m} n(t)\sin(\omega_1 t+\phi)\sin(\omega_2 t)\,dt, \end{aligned} \tag{19}$$

where T_m is the average signal sampling (integration) time determined by the RC time constant of the low-pass filter,[16,17] which should be set larger than $T=\max(2\pi/\omega_{1,2})$ in order to obtain an undistorted (''true'') output. It is seen from Eq. (19) that the final output of the LIA contains two terms: the first term is the contribution from the harmonic signal; the second term is the noise contribution to the demodulated output. Owing to the orthogonality of sine-wave functions, the first term is always zero if $\omega_1 \neq \omega_2$. However, if $\omega_1=\omega_2(\equiv\omega)$, the average value of the first term yields a dc output proportional to the Fourier coefficient of the periodic signal, the frequency of which is *exactly* that of the reference. Equation (19) can thus be rewritten as

$$\begin{aligned} V_{\mathrm{LIA}}(\omega,t) &= \frac{1}{2}A_s A_r \cos\phi + (A_r/T_m)\int_0^{T_m} n(t)\sin(\omega t+\phi) \\ &\quad \times \sin(\omega t)\,dt; \quad \omega_1=\omega_2(\equiv\omega). \end{aligned} \tag{20}$$

Equation (20) shows that the LIA output, *for an input signal of the same frequency as the reference signal*, is proportional to the oscillating input signal vector component $A_s \cos\phi$. With the help of the phase shifter (common in modern two-channel LIAs, the amplitude A_s and the phase ϕ of the signal can be simultaneously determined if the reference amplitude A_r is known.[15] Equation (20) further indicates that in the presence of noise, the output signal is accompanied by a noise-integral, T_m-dependent term. The degree of noise reduction depends on the nature of the input noise. For white noise (high-frequency random fluctuation), the averaged value of the noise term is virtually zero, if the integration time T_m is long enough when compared with the signal wave form repetition period $T_0=2\pi/\omega$. If the input noise is a slow signal drift (usually due to electronics), it can partially pass through the lock-in amplifier, depending on the relative values of the integration time constant T_m and the inverse of the noise drift rate. For a given T_m, the slower the drift, the larger the amount passing through the LIA. Theoretically, the output of a LIA may be completely free of white noise *and* slow noise drift, provided the integration time is infinite. However, the larger the integration time, the slower the LIA response. Therefore, in practice a compromise is sought, and noise reduction can be controlled by employing the appropriate T_m as shown in Eq. (20). As a result, the actual output of a LIA is always accompanied by noise which is, however, much smaller than the input noise. For the low-pass filter, a very good approximation of the integration time is the operator-controlled instrumental time constant of the LIA.[17] Turning to the PPE signal-generation problem, the noised PVDF sensor signal voltage, $V_{\mathrm{PVDF}}(\omega,t)$, given explicitly in Eq. (16), is directly input to the LIA. Thus, the demodulated output signal is

$$V_{\mathrm{LIA}}(\omega)=(1/T_m)\int_0^{T_m} V_{\mathrm{PVDF}}(\omega,t)\sin(\omega t)\,dt. \tag{21}$$

IV. EXPERIMENTAL INVESTIGATION OF THE NATURE OF LASER INTENSITY-FLUCTUATION NOISE

Before we go to the detailed theoretical simulation, we first introduce the schematic of the experimental system used for destructive interferometric PPE detection[2–4] on which the present noise analysis is based. Figure 2 shows a simplified experimental setup. Two laser beams, which are split off of a single He–Ne laser (Model 05-LHP-925, Melles Griot) and modulated at the same frequency, are incident directly onto the front and rear surfaces of a PVDF detector, as shown in Fig. 1. The relative intensities of the two beams can be adjusted by a linear intensity attenuator, and the phase shift between the two beams is precisely controlled by adjusting a

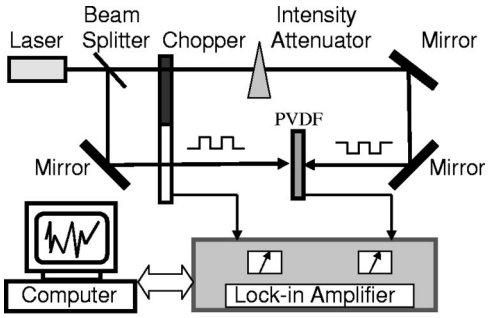

FIG. 2. Schematic diagram of the experimental PPE setup for single-beam and two-beam measurements.

mechanical chopper (EG&G Model 192). The PPE signal from the PVDF is fed into a lock-in amplifier (EG&G, Model 5210), which is controlled by a PC. Single-beam or two-beam (interferometric) thermal-wave measurements can be easily performed by simply blocking or unblocking the rear laser beam, respectively. Only laser-related noise will be considered in the theoretical simulation, since this is the main source of signal-generation difference between the foregoing two types of measurements.

To understand the noise characteristics of the PPE interferometric system, a description of the laser-intensity fluctuation (noise) components $N_1(\tau)$ and $N_2(\tau)$, which appear in Eq. (16), is necessary. Figure 3 shows a typical intensity output of the He–Ne laser source measured with a photodiode to observe output beam stability over a long period. The intensity was monitored after a 2 h warmup. The intensity is seen to fluctuate with time about a mean value and the variations can be considered to constitute ''noise'' accompanying a constant intensity output. In view of Fig. 3, three types of noise can be identified:

(1) *dc drift*. This instability usually arises mainly from changes in the operating temperature of the laser plasma tube over the entire duration of the measurement. It usually increases slowly and steadily with time.
(2) *Low-frequency oscillation* V_{LF}. Over the measurement time of several hours, the output intensity oscillates very slowly. This noise may arise from several factors, such as changes in ambient temperature and electrical processes in the laser power supply. It is seen that this noise variation is much larger than the dc drift.

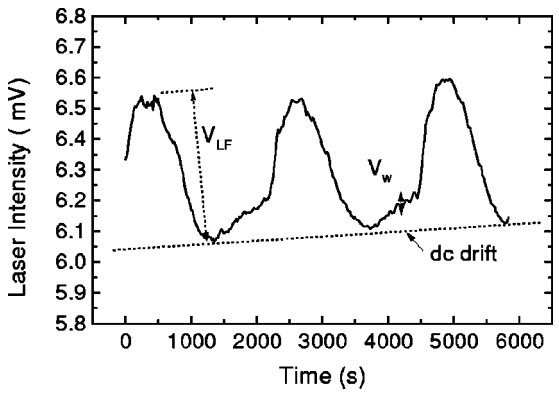

FIG. 3. Experimental intensity measurement of a He–Ne laser.

(3) *White noise* V_W. This is the most commonly encountered noise in all optical and electronic measurements,[18] including PPE detection. By ''white noise'' we mean a high-frequency random fluctuation with zero mean. This noise is mainly due to thermal and/or shot noise in electronic components and circuits, as well as to spontaneous emission and mode hopping in the laser cavity.[19]

Comparing the contributions from the three aforementioned noise sources in Fig. 3, it is clear that the dc drift and the low-frequency oscillation V_{LF} dominate the overall noise characteristics of the laser output. White noise V_W, on the other hand, contributes very little to the overall noise. In addition, the discussion in Sec. III B above shows that the LIA is more effective in reducing or eliminating white noise than low-frequency oscillations and dc drifts. Therefore, it is important to understand the extent of the noise reduction capabilities of a LIA with respect to the latter two noise sources, i.e., dc drift and low-frequency drift. Contributions from white noise will be neglected in the following discussion.

V. SEMIEMPIRICAL SIMULATIONS OF NOISE SOURCES IN PPE OUTPUT

Based on the experimental laser response, the overall noise from the laser source of the PPE instrument in Fig. 3 can be expressed as a summation of dc drift and low-frequency oscillation drift. The dc drift can be written as a linear function of time, while the low-frequency drift can be represented by a sum of sinusoids of different frequency components.[15,18] Therefore, the overall noise $N(t)$ and the total intensity output $I(t)$ (noise included) from the laser can be analytically expressed as

$$N(t)=C_0 t+\sum_n C_n \cos(2\pi f_n t+\theta_n) \tag{22}$$

and

$$I(t)=I_0+N(t). \tag{23}$$

In Eq. (22), the first term represents the dc drift and the second term is the low-frequency periodic drift, Fig. 3. C_0 (unit: s^{-1}) and C_n are constants. f_n (unit Hz) and θ_n (unit: rad) are the frequencies and the phases, respectively, of the noise components. In Eq. (23), I_0 represents a constant intensity output. Figure 4 shows a theoretical simulation of the laser output using Eq. (23). The parameters used in the simulation are: $I_0=610$ (a.u.), $C_0=0.16$, and $n=5$. For the various frequency components ($n=1-5$), $C_n=10-0.6n$; $f_n=0.003\,05(n-1)^2$; and $\theta_n=0.2\pi n$. These parameters give a generalized theoretical intensity output similar to the experimental results of Fig. 3, in the sense that the noise time record features a monotonic dc drift and an adjustable low-frequency oscillation with a magnitude of 48 a.u.

To simulate the output of the PVDF detector, followed by the LIA output in the double-beam configuration of Fig. 2 and in the framework of Eq. (23), we recall that fully de-

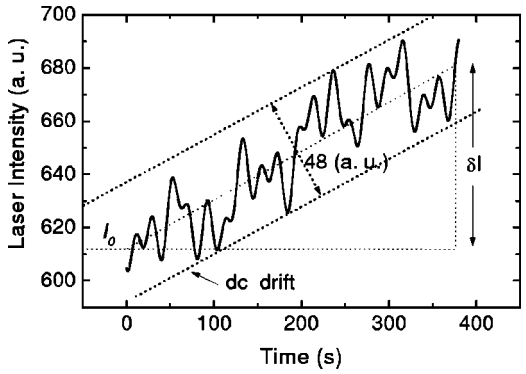

FIG. 4. Theoretical simulation of intensity fluctuations of a laser beam.

structive thermal-wave interference occurs when the intensities of the two beams are adjusted to be equal, and the phase shift between the two beams is adjusted by the mechanical chopper, such that the phase shift between the front beam and the rear beam is exactly 180°. This physically means that the front and rear beams are allowed to pass through the chopper and impinge onto the respective surfaces of the PVDF element alternately. This type of beam modulation scheme amounts to a zero sum thermal-wave flux out of the PVDF film at all times, as the front outflux during the *off* half cycle is always precisely balanced out by the back influx during the *on* half cycle. The result is a constant thermal content of the film and yields zero LIA output, which is interpreted as completely destructive PPE thermal-wave interference.[2] Therefore, the noised intensities of the front and the rear beams in Eq. (16) can be represented as

$$I_1+N_1(\tau)=\frac{1}{2}\left[I_0+C_0\tau+\sum_n C_n\cos(\omega_n\tau+\theta_n)\right], \quad (24)$$

$$I_2+N_2(\tau)=\frac{1}{2}\left\{I_0+C_0\left(\tau+\frac{1}{2}T_0\right)+\sum_n C_n\cos\left[\omega_n\left(\tau+\frac{1}{2}T_0\right)+\theta_n\right]\right\}. \quad (25)$$

In Eq. (25), $T_0(=2\pi/\omega)$ is the modulation period of the mechanical chopper. Substituting Eqs. (24) and (25) into Eq. (16) and the result into Eq. (21), the output signal from the PVDF detector before the LIA, and the demodulated signal output from the LIA may be calculated numerically. To simplify the two-dimensional numerical integral in Eq. (21), first the one-dimensional integral of Eq. (16) may be calculated by substituting Eqs. (24) and (25) into Eq. (16). This equation then becomes

$$\begin{aligned}V_{\mathrm{PVDF}}(\omega,t)=Q(\omega)\frac{\alpha_p}{k_p}\Bigg\{&\frac{P_1I_1\sin\omega t+P_2I_2\sin(\omega t+\varphi)-P_2I_2\sin\varphi}{\omega}\\&+C_0\Bigg[\frac{2t[P_1\sin(\omega t)+P_2\sin(\omega t+\varphi)]+P_2T_0[\sin(\omega t+\varphi)-\sin\varphi]}{4\omega}\\&+\frac{P_1(\cos\omega t-1)+P_2[\cos(\omega t+\varphi)-\cos\varphi]}{2\omega^2}\Bigg]\\&+\sum_{i=1}^{2}\sum_n P_iC_n\Bigg[\frac{\sin[(\omega_n-\omega)t]\cos(\theta_n-\Phi_{i-})+\{\cos[(\omega_n-\omega)t]-1\}\sin(\theta_n-\Phi_{i-})}{4(\omega_n-\omega)}\\&+\frac{\sin[(\omega_n+\omega)t]\cos(\theta_n+\Phi_{i+})+\{\cos[(\omega_n+\omega)t]-1\}\sin(\theta_n+\Phi_{i+})}{4(\omega_n+\omega)}\Bigg]\Bigg\},\end{aligned} \quad (26)$$

where $\omega_n=2\pi f_n$ is the angular frequency of the nth noise component, $I_1=I_2=0.5I_0$, and

$$\Phi_{i+,i-}=\begin{cases}0, & i=1\\ \omega_n(T_0/2)\pm\varphi, & i=2.\end{cases} \quad (27)$$

Equation (26) explicitly gives the time dependence of the output signal from a PVDF detector in the presence of noise wave forms of the type described by Eq. (22) from both incident laser beams. The LIA signal output can now be calculated by substituting $V_{\mathrm{PVDF}}(\omega,t)$ in Eq. (26) into Eq. (21).

A. Simulation of noised single-beam PPE output signal

Equation (26) holds for the general case of Fig. 1, which includes the front and rear incident laser beams, phase shifted by φ. However, if the rear beam is absent, i.e., $I_2=0$, then $N_2(\tau)=0$, or directly $P_2=0$. Equation (26) now reduces to the single-beam case

$$V_{\mathrm{PVDF}}(\omega,t)=Q(\omega)\frac{\alpha_p}{k_p}P_1\left\{\frac{I_1\sin\omega t}{\omega}+C_0\left[\frac{2t\sin\omega t}{4\omega}+\frac{(\cos\omega t-1)}{2\omega^2}\right]\right.$$
$$+\sum_n C_n\left[\frac{\sin[(\omega_n-\omega)t]\cos\theta_n+\{\cos[(\omega_n-\omega)t]-1\}\sin\theta_n}{4(\omega_n-\omega)}\right.$$
$$\left.\left.+\frac{\sin[(\omega_n+\omega)t]\cos\theta_n+\{\cos[(\omega_n+\omega)t]-1\}\sin\theta_n}{4(\omega_n+\omega)}\right]\right\}. \quad (28)$$

Figure 5 shows the single-beam modulated PPE signal from the PVDF as a function of time before the LIA. In the calculation, the modulation frequency $f=10$ Hz, $I_1=0.5I_0$, and both constants related to the instrumental factor, $Q(\omega)\alpha_p/k_p$, and P_1 were assumed to be unity. All other parameters are the same as in Fig. 4. Note that the PVDF output signal is periodic, with frequency equal to the modulation frequency. The structure of this periodic signal is magnified in Fig. 5(b), showing the thermal wave between 0 and 2 s. The noise envelope, including the dc drift and the low-frequency oscillation, can be seen as the amplitude fluctuation in Fig. 5(a). The PVDF signal is then input to the LIA, the output of which is obtained by performing the integration in Eq. (21). The integration time T_m was set to 1.0 s in the calculation, which is our experimental LIA filter time constant. The demodulated signal output from the LIA is shown in Fig. 6. Both dc drift and low-frequency noise are seen to pass through the LIA without significant reduction. This noise envelope, which was assumed to originate at the incident laser beam, (Fig. 4) comprises approximately 7.4% of the instrumental output, compared with 7.8% in the incident beam of Fig. 4. A similar conclusion applies to the dc drift: The ratio of the amplitude of the dc drift δV over the signal level V_0 in the final output (11.2%) is basically the same as that $(\delta I/I_0)$ in the incident beam (11.4%).

B. Simulation of noised two-beam (interferometric) PPE output signal

In the case of two-beam fully destructive interference, we have $I_1=I_2=0.5I_0$, and the phase shift $\varphi=180°$. By using the same parameters and the same normalized constants as with the single-beam mode, i.e., $Q(\omega)\alpha_p/k_p=P_1=P_2=1$, we obtain the results shown in Fig. 7, the PVDF signal calculated from Eq. (26), and in Fig. 8, the LIA demodulated output signal calculated from Eq. (21) using Eq. (26) in the integrand. The PVDF signal in the two-beam mode is also periodic at the frequency $f=\omega/2\pi$. Details of the oscillation in Fig. 7(a) between 0 and 2 s are magnified in Fig. 7(b). Inspection of Figs. 5 and 7 immediately shows that the large PVDF single-beam signal has been suppressed by ~3 orders of magnitude in Fig. 7. Furthermore, the dc drift envelope in Fig. 5 has disappeared from Fig. 7. Further quantitative comparison between the single-beam and two-beam cases can be made by examining the final demodulated signals from the LIA, Figs. 6 and 8, respectively. The two-beam LIA output signal is completely free of the dc drift, in sharp contrast with the single-beam case. The amplitude of the low-frequency two-beam noise is reduced by about 120 times less than the single-beam noise. In agreement with our experiments, it is concluded that the background signal level of the

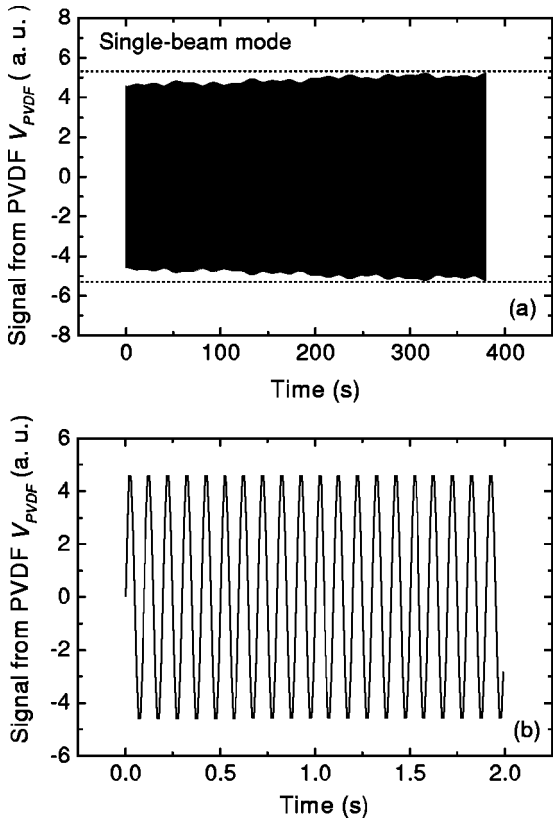

FIG. 5. (a) Signal output of the PVDF detector (LIA input), single-beam; (b) details of (a) showing the periodic oscillation between 0 and 2 s.

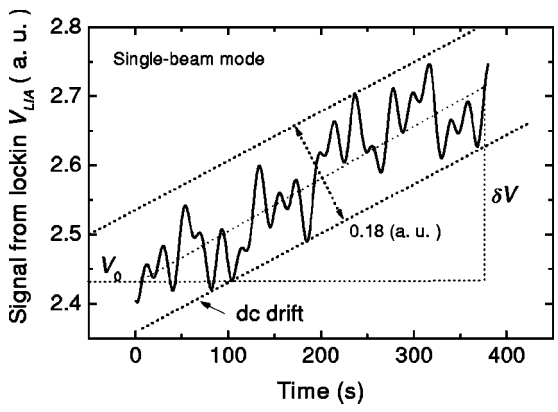

FIG. 6. Signal output from a lock-in amplifier in single-beam mode.

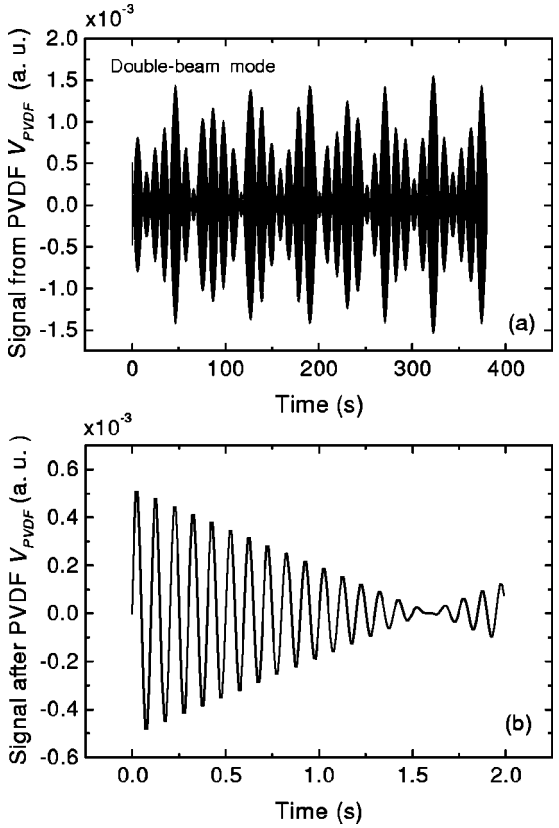

FIG. 7. (a) Signal output of the PVDF detector (LIA input) in two-beam fully destructive interferometric mode; (b) magnified details of (a) showing the periodic oscillation between 0 and 2 s.

single-beam case is nearly completely cancelled out in the two-beam destructive interferometric mode. The latter is shown to be a powerful differential measurement technique for suppressing large baseline photothermal signals, as well as electronic dc drifts and low-frequency laser-generated noise, using only a single PVDF detector.

C. The effect of LIA sensitivity scales on PPE white noise

In the foregoing discussion, white noise from laser-beam fluctuations (e.g., pointing noise) was ignored, considering its very small contribution to the overall signal output noise

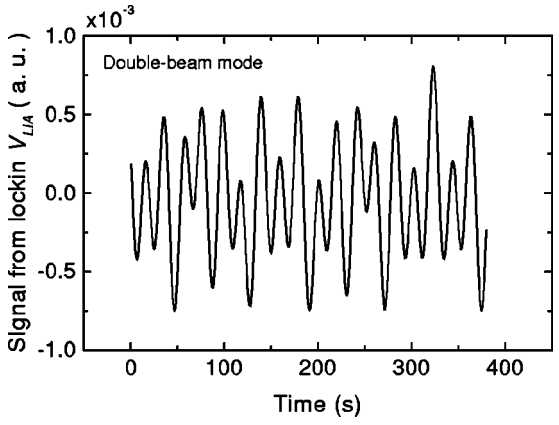

FIG. 8. LIA signal output in the two-beam destructive interferometric mode.

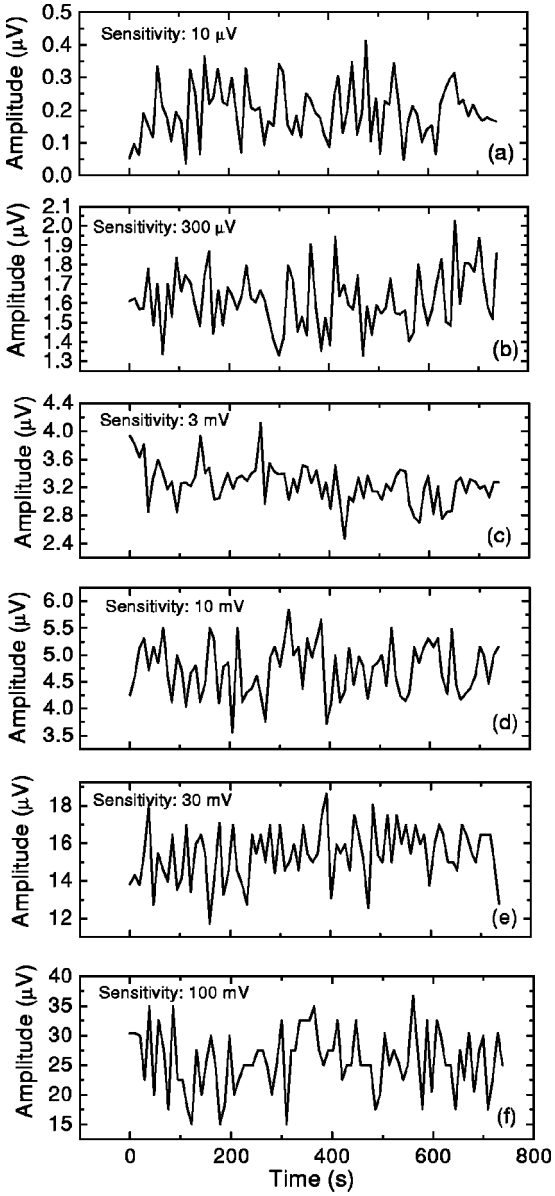

FIG. 9. Experimental noise level of EG&G 5210 LIA at various sensitivity scales.

based on experimental observations. Neglecting this type of noise can be further rationalized by considering that a LIA is a much more efficient filter for suppressing white noise than dc drift or low-frequency noise.[14,17] In this section, white noise from the LIA itself and its contribution to the overall system noise will be discussed as a function of the amplification stage (sensitivity scale) selected for a given PPE measurement. As a consequence of the nature of the single-beam and the two-beam fully destructive interferometric measurements, very different LIA sensitivity scales are used for each measurement. In the former case, as shown in Fig. 6, a much lower sensitivity scale must be used to match the large baseline signal. Different sensitivity scales of a LIA introduce different levels of white noise to the measurements due to different amplification stages. Figure 9 shows actual noise time records of the same input using different sensitivities of the LIA (EG &G, Model 5210). The signal source used in the experiment is a PVDF thin film detector (no incident

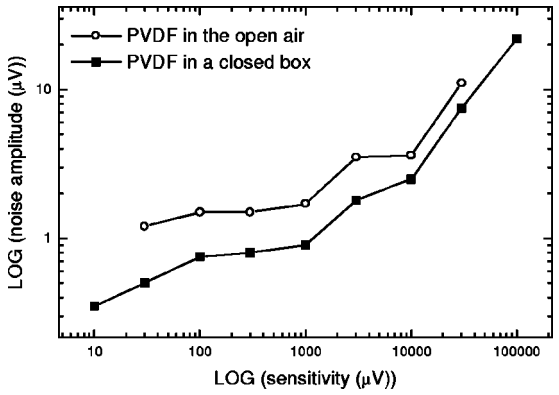

FIG. 10. Experimental noise amplitude of the LIA output vs LIA sensitivity.

laser beam), installed in a closed box to reduce external optical and thermal noise. For such a noise source the LIA output represents the noise limit of the measurement system. It can be seen that the noise amplitude increases monotonically with the LIA sensitivity scale. To quantify this relationship, the experiment was repeated by using a different noise source. The PVDF detector was taken out of the closed box and into the open air. Plots of the LIA noise amplitude versus LIA sensitivity scale for both experiments are shown in Fig. 10. As expected, the unshielded PVDF produces higher overall output noise. In view of the fact that the noise source remained unchanged for all LIA sensitivity ranges, the observed noise increase can only originate in the amplification electronics of the LIA itself at each sensitivity scale. Indeed, the LIA sensitivity is set by adjusting the gains of both input and output amplifiers. The input amplifiers are ac coupled, but the output amplifiers are dc coupled.[13] dc coupled amplifiers commonly exhibit thermal noise and dc drift with time, the effects of which are suitably amplified as the dc gain increases. Changing the LIA sensitivity results in redistribution of ac and dc gains between the signal channel (ac amplifier) and the output (dc amplifier).[13,14] For a lower sensitivity, the ac gain in the signal channel is reduced, while the dc gain in the output channel is increased (amplified) accordingly, so as to keep the overall gain the same. Therefore, a lower LIA sensitivity results in a larger noise. In most of our measurements, the signal levels were, typically, 3–10 mV (single beam) and 0.5 μV (destructive interferometric two beam). Consistent with Fig. 10, the PPE single-beam white noise level caused by lower sensitivity of the LIA was ~six times higher than that of the two-beam case, using 10 mV and 10 μV sensitivity scales, respectively.

VI. PPE DESTRUCTIVE INTERFEROMETRIC DETECTIVITY ENHANCEMENT

The detectivity enhancement in two-beam destructive PPE interferometry is based on experimental evidence.[3,4] The experimental setup is as shown in Fig. 2. Experiments were conducted in the following sequence: Before turning the laser beam onto the PVDF, the background noise of the system was measured using a lock-in sensitivity of 10 μV. This noise consists of contributions from detector and amplifier represented by the first four terms in Eq. (1). The LIA output is shown in Fig. 11(a). Then, the two oppositely directed laser beams were introduced and the relative intensity was adjusted to the fully destructive interferometric mode. The LIA output was on the same sensitivity scale (10 μV), shown in Fig. 11(b). Subsequently, the rear incident beam was blocked and the output was recorded in Fig. 11(c). In this case, the sensitivity of the lock-in was changed to 10 mV to match the large signal. Comparing Figs. 11(a), 11(b), and 11(c) it is concluded that the LIA output signal in the fully destructive configuration, Fig. 11(b), was virtually at the instrumental noise baseline, in the range 0.6–0.7 μV. This is an increase of only about 0.2 μV compared to the noise output without laser excitation, Fig. 11(a), in the range of 0.4–0.5 μV. This noise increase is due to the introduction of the two out-of-phase laser beams and demonstrates the beneficial effect of baseline suppression. In Fig. 11(c), a large LIA output (~2.9 mV) is accompanied by an increase in noise level to a mean value of ~30 μV. This shows that the noise level originated from laser-induced fluctuation in the single-beam mode is about 150 (=30 μV/0.2 μV) times larger than in the interferometric mode. This experimental result is in good agreement with the foregoing semiempirical theoretical analysis. Recall that the input noise levels assumed in the theoretical development were chosen so as to match experimentally observed noise. The analysis predicts a 120-fold increase of the laser-induced low-frequency noise in the single-beam mode (Fig. 6) over the two-beam mode (Fig. 8). It is seen from Figs. 11(b) and 11(c) that the overall noise level (including all types of noise: laser-induced fluctuation noise, system background noise, and white noise from the LIA) in the single-beam mode is more than 40 times (=30 μV/0.7 μV) higher than that in the two-beam interferometric mode. Therefore, the NEP of the interfero-

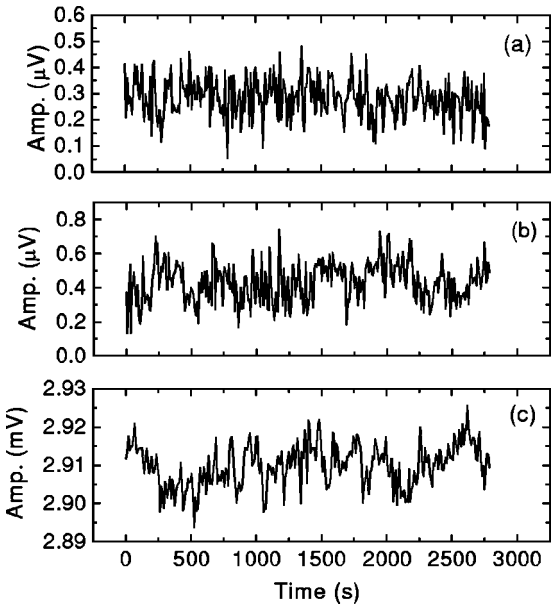

FIG. 11. PPE demodulated signal output and the overall system noise evaluation for various instrumental operation modes: (a) system background noise, laser beams blocked; (b) signal output and accompanying noise in fully destructive interferometric mode, with two laser beams on; (c) signal output and accompanying noise with a single laser beam on.

metric configuration is about 40 times less than that in the single-beam method. Accordingly, the detectivity, D^*, Eq. (3), is enhanced by the same factor.

It is possible to correlate the enhancement of D^* to the figure of merit (FOM) of the system. For the instrument in Fig. 2, the system FOM is defined as the ratio of the one-beam to the two-beam PPE signal amplitude. According to experimental results in Fig. 11, the overall noise output is related to the signal amplitude for a given configuration. For the single-beam outputs

$$\Delta V_{N1} = \zeta S_1, \tag{29}$$

where S_1 is the signal amplitude, and ζ is the percentage of the system noise output (largely laser-induced low-frequency noise, Fig. 3). In the two-beam destructive interferometric mode, the baseline suppression essentially eliminates all but the residual low-frequency noise as shown in Fig. 8. This overall noise level can be taken as the minimum detectable signal level, S_2, i.e.,

$$\Delta V_{N2} = S_2. \tag{30}$$

Therefore, the detectivity enhancement ΔD^* under destructive interferometric operation is

$$\Delta D^* = \zeta \times (S_1/S_2) = \zeta \times \mathrm{FOM}. \tag{31}$$

This result has been validated in the case of a destructive interferometric PPE hydrogen sensor.[4] In that case, we employed a PVDF thin film as the transducer. The PVDF is coated with NiAl metals on one surface (reference coating) and palladium metal on the other (H_2 sensitive coating). By employing the fully destructive thermal-wave interferometric mode, we detected a trace hydrogen level of about 100 ppm if a 53.4 nm palladium coating is used. As a comparison, the measurement was also conducted in the single-beam mode, which shows a detection limit of about 0.2% hydrogen concentration. From our measurements, the coefficient $\zeta = 0.007\,43$, as determined from single-beam results. The experimental FOM was 3300. Therefore, Eq. (31) yields a 24-fold enhancement in D^*, which compares well with the observed $\Delta D^* = 20$.

VII. DISCUSSION

Based on experimental observations, a semiempirical quantitative PPE instrumental noise and detectivity theory has been developed to compare thermal-wave destructive interferometric and conventional single-beam operations. The observed significant noise suppression in the interferometric scheme has been shown to be due to effective LIA filtering of the laser-induced dc drift and low-frequency noise. The dc drift is essentially completely suppressed, whereas the low-frequency noise is decreased by more than 120-fold over that of the single-beam mode. White noise introduced by a LIA is also reduced, under interferometric PPE operation, typically more than six fold. A FOM for the PPE interferometer was established, its relationship with the instrumental detectivity was found, and the detectivity enhancement was calculated.

As a consequence, the photopyroelectric thermal-wave interferometer provides a sensitive, LIA-signal baseline-suppression method. The LIA effectively suppresses the overall instrumental noise due to laser-source beam intensity fluctuations, as well as its own internal white noise through optimized sensitivity scale selection. Such an optimization becomes possible as a result of the baseline suppression. It is expected that the destructive PPE interferometer will become a useful tool for optical, scanning imaging, and thermophysical studies, including novel gas sensors.

ACKNOWLEDGMENTS

The authors would like to thank Dr. Stefano Paoloni (University of Rome) for valuable discussions. The support of Natural Sciences and Engineering Research Council of Canada (NSERC) through a research grant is gratefully acknowledged.

[1] A. Mandelis and M. M. Zver, J. Appl. Phys. **57**, 4421 (1985).
[2] C. Wang and A. Mandelis, J. Appl. Phys. **85**, 8366 (1999).
[3] C. Wang and A. Mandelis, Rev. Sci. Instrum. **70**, 2372 (1999).
[4] C. Wang, A. Mandelis, and J. Garcia, Sensors Actuators B **60**, 228 (1999).
[5] E. H. Putley, in *Semiconductors and Semimetals*, edited by R. K. Willardson and A. C. Beer (Academic, New York, 1970), Vol. 5, Chap. 6, p. 268.
[6] G. A. Burdick and R. T. Arnold, J. Appl. Phys. **37**, 3223 (1966).
[7] J. Cooper, Rev. Sci. Instrum. **33**, 92 (1962).
[8] Van der Ziel, *Noise in Measurement* (Wiley, New York, 1976), pp. 99–101.
[9] J. N. Zemel, in *Solid State Chemical Sensors*, edited by J. Janata and R. J. Huber (Academic, New York, 1985), Chap. 4.
[10] P. C. D. Hobbs, Proc. SPIE **1376**, 216 (1990).
[11] G. C. M. Meijer and A. W. Herwaarden, *Thermal Sensors* (Institute of Physics, Bristol, 1994).
[12] J. V. Beck, K. D. Cole, A. Haji-Sheikh, and Litkouhi, *Heat Conduction Using Green's Functions* (Hemisphere, Washington, DC, 1992), pp. 43, 492.
[13] The Analog Lock-in Amplifier, Technical Note TN1002, Princeton Applied Research Corp., Princeton, NJ (1999); Technical Description in *Instruction Manual for EG&G 5210* (1987), Chap. 3.
[14] M. L. Meade, *Lock-in Amplifiers: Principles and Applications*, IEEE Electrical Measurement series 1 (Peregrinus, Stevenage, Herts, England, 1983).
[15] A. Mandelis, Rev. Sci. Instrum. **65**, 3309 (1994).
[16] G. L. Miller, J. V. Ramirez, and D. A. H. Robinson, J. Appl. Phys. **46**, 2638 (1975).
[17] T. H. Wilmshurst, *Signal Recovery from Noise in Electronic Instrumentation*, 2nd ed. (Adam Hilger, Bristol, 1990), p. 72.
[18] B. P. Lathi, *An Introduction to Random Signals and Communication Theory* (International Textbook, Scranton, PA, 1968), Chap. 3, p. 209.
[19] K. I. Iga, *Fundamentals of Laser Optics* (Plenum, New York, 1994), p. 223.